Desalination and Water Treatment
www.deswater.com

doi: 10.5004/dwt.2022.28453

260 (2022) 52–62
June

Bubble-particle collision efficiency in rotating dissolved air flotation in paper-recycling wastewater treatment: experiments and modeling

Abbas Hasannattaj Jelodar[a], Hasan Amini Rad[a,*], Seyed Mehdi Borghei[b], Manuchehr Vossoughi[b], Rahmatollah Rouhollahi[c]

[a]*Babol Noshirvani University of Technology, Faculty of Civil Engineering, 4714871167 Babol, Iran, Tel. +98 911 112 1477; email: h.a.rad@nit.ac.ir, https://orcid.org/0000-0002-0622-3681 (H. Amini Rad), Tel. +98 911 117 1926; email: nattaj2008@yahoo.com, https://orcid.org/0000-0002-7344-6674 (A. Hasannattaj Jelodar)*
[b]*Sharif University of Technology, Faculty of Chemical Engineering, 1458889694 Tehran, Iran, Tel. +98 912 113 0394; email: mborghei@sharif.edu, https://orcid.org/0000-0002-9825-9832 (S.M. Borghei); Tel. +98 21 6616 4104; email: vosoughi@sharif.edu, https://orcid.org/0000-0002-1238-4887 (M. Vossoughi)*
[c]*Babol Noshirvani University of Technology, Faculty of Basic Sciences, 4714871167 Babol, Iran, Tel. +98 911 313 1363; email: r.rouhollahi@nit.ac.ir*

Received 16 December 2021; Accepted 29 March 2022

ABSTRACT

Paper-recycling mills are serious environmental threats due to their high water consumption and highly polluted wastewater. Particles are the most common issue of paper-recycling wastewater, and their removal is of particular interest for recycling. Rotating dissolved air flotation (RDAF) is a system for separating particles, and the mixing zone of this system, where particles collide with air bubbles, is the most important part. As a widely used system in various industries, RDAF has rarely been investigated in the literature in terms of its optimization and efficiency improvement. In general, RDAF processes are basically the same as those of conventional dissolved air flotation (DAF) systems; thus the results of RDAF can be applied to other DAF systems. In this work, the mixing zone of a full-scale RDAF for the paper-recycling mill wastewater treatment was investigated to predict particle-bubble collision efficiency, consisting of both particle-bubble transport and attachment, and the diameter of the formed particles in different turbulence conditions. ANSYS CFX R18.0, mathematical modeling, and experimental analysis were simultaneously conducted in this research. Based on experimental operation, four scenarios including flow rates and the discharge condition of effluent into the mixing zone were studied. Bubbles with sizes of 60, 80, and 100 μm, the turbulences were calculated. The obtained particle-bubble collision efficiencies indicated the diameter of output particles ranged from 50 to 300 μm. Also, the static light scattering test was performed to determine the particle sizes. The modeling and experimental results both showed that the collision efficiency was higher with the production of larger particles when valves #3 and #4 were opened in the mixing zone.

Keywords: Bubble-particle; Collision efficiency; Modeling; Paper-recycling wastewater; Particle size; Rotating dissolved air flotation

* Corresponding author.

1. Introduction

The wastewater of paper-recycling mills includes very fine pulp and paper particles. Collision and separation of particles in paper-recycling mills are important from the environmental and economic aspects. Rotating dissolved air flotation (RDAF), known as "Krofta", is a widely used system for paper-recycling wastewater treatment that consists of a circular tank with a rotating paddle for cumulating the particles [1,2]. The optimization of RDAF, similar to other DAFs, can be discussed in terms of reaching a more efficient bubble-particle collision and coagulation [3], obtaining higher-quality wastewater and better particle removal [4–6], and using new pieces of equipment replacing old ones [7]. The collision of particles and their attachment to one another to form a greater floc is the basis of flocculation [8–10]. Several research works show the significant role of the air bubbles' behavior and concentration and their collisions with particles in optimization [11–17]. Computational fluid dynamics has been used as a proper tool to simulate the behavior of single- or multi-phase flows [18–21]. This technique has been extensively employed for the simulation of the interactions of fluid phases in DAF [22–25]. Also, k–ε is a model for turbulence that has the most applications and gives results that are more consistent with test results [26,27]. On the other hand, another approach for the simulation of bubble-particle interaction and particle size in DAF is mathematical modeling [28–30]. A study on paper-recycling wastewater showed that the intensity of turbulence is effective on particle removal efficiency [31–33]. Moreover, micro turbulences affect particle flotation more significantly [34–36]. Also, tank hydrodynamic conditions and flotation rates in DAF interact and affect the particle removal efficiency [37–41]. Based on a decade of experimental operation, it was observed that with the change of flow conditions (scenario), the particle removal efficiency changes in the separation zone. Particle removal efficiency can depend on the particle diameter in paper-recycling wastewater. The function of the separation zone depends directly on the performance of the mixing zone. Therefore, the most important purpose of this study was to investigate the collision-attachment between particles and bubbles, namely the particle-bubble collision efficiency, caused by turbulence changes in the mixing zone. To address this subject, the mixing zone of a full-scale RDAF used for paper-recycling mill wastewater treatment in Mazandaran, Iran, was investigated using ANSYS CFX R18.0, mathematical modeling, and experiments.

2. Materials and methods

Here, a full-scale RDAF applied for treating the wastewater of a paper-recycling mill in Rangin Kaghaz-e-Khazar Co., Mazandaran, Iran, was considered. RDAF consists of a set of discharge valves and a skimmer that rotate together in an iron tank in the form of a donut. The outer diameter and height of this donut-shaped tank are 4 m, and 60 cm, respectively. Four discharge valves, 8 cm in diameter and 30 cm in height, with specified spacing, discharge the wastewater and compressed air (bubbles) into the second mixing zone. The main wastewater transfer pipe is divided into four discharge valves, namely valve #1, #2, #3, and #4, in order. Fig. 1 schematically shows an RDAF together with the inlet and outlet and meshing. Air bubbles are provided in this system by using a compressor to supply a portion of the wastewater to an air-saturator unit and then inject it into the main pipe. Different situations for the wastewater discharge into the RDAF's mixing zone are shown in Table 1. Scenarios were selected from a decade of experimental operation, based on the observation that with the opening and

Table 1
Different scenarios for the discharge of wastewater into the mixing zone

Opened valves	Total flow rate (L/s)	Velocity in valves (m/s)
1,2,3,4	6.15	0.415
1,2,3,4 (normal)	7.7	0.514
1,2	7.7	1.01
3,4	7.7	1.01

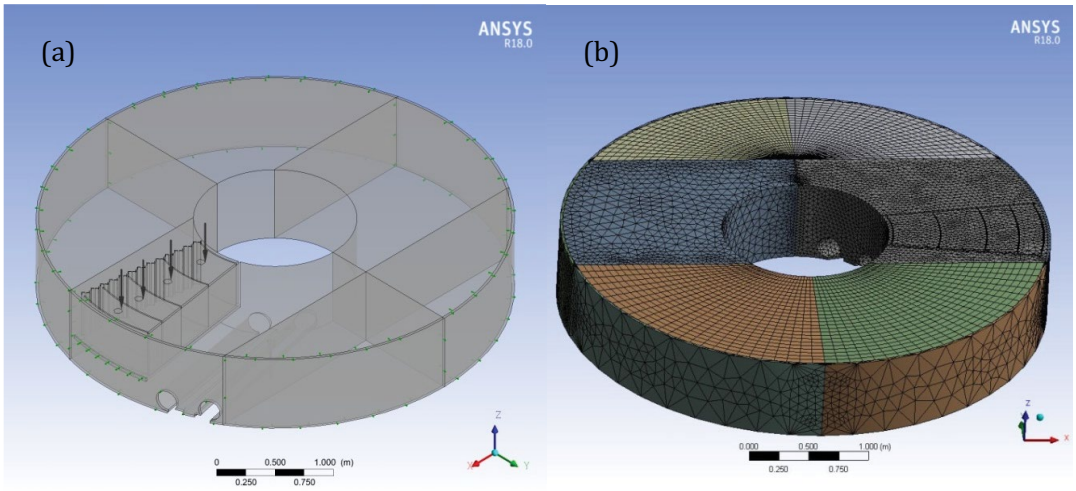

Fig. 1. (a) RDAF schematic of inlet and outlet and (b) meshing.

closing of the valves, the effluents will be darker or brighter, as stated by the operator. Finding the cause of this issue became the base of this study. Four scenarios including flow rates and the discharge condition of effluent into the mixing zone were studied. Fig. 2 shows a schematic illustration of the RDAF, in which the black line from the air injection point to the mixing zone shows the study domain, which is the particle collision zone. The mixing zone in this study consists of two parts: from the air injection point in the main pipe to the outlet of valves and from the outlet of valves to baffles. After the passing of flow through the iron bars, the flow enters the separation zone in which particles float and become separated from the wastewater. The approach used in this research consists of three parts. In the first part, by using equations for the particle-bubble collision in the main pipe based on mass balance, the particle-bubble collision efficiency model was obtained. In the second part, ANSYS CFX R18.0 software was employed to simulate the model and obtain some of its parameters. The developed RDAF mesh in ANSYS CFX consisted of 317076 grids. A transient flow with a time step of 0.05 was taken into account. The third part involved particle analysis to experimentally validate the model and ANSYS CFX results. The particle size test was performed extensively for the three scenarios by the static light scattering (SLS) to determine the particle sizes. Sampling was performed at three different points in the RDAF: after the valves, the baffles (second mixing zone), and the collector (output), respectively. For further investigation, two samples were taken at slow and rapid rotating speeds of the valves. The rotating time was 480 s at a slow speed and 80 s at a rapid speed. After transferring the collected samples to the laboratory, based on standard time intervals for analysis, the tests were conducted [42].

2.1. Mathematical model

The general equation for the particle growth rate (N_{ij}) in terms of a second-order particle-bubble collision rate between particles with i and j sizes is as follows [1,19,43]. Particle-bubble collision efficiency in this study includes particle-bubble transported and attachment.

$$N_{ij} = \alpha_{ij}\beta_{ij}n_i n_j \tag{1}$$

where N_{ij} is the overall particle growth rate, β_{ij} is the collision mechanism, α_{ij} is the collision efficiency factor ($0 < \alpha_{ij} < 1$), and $n_i n_j$ is the particle collision rate. Mass balance is considered as the plug flow, and dispersion is neglected [44,45]. The flow rate $Q + Q_r$ is constant, and the particle balance statement is expressed by Eq. (2) [1]:

$$\frac{\partial n_p}{dt}\left(A\Delta L\right) = \left(Q+Q_r\right)n_p - \left(Q+Q_r\right)\left(n_p+\Delta n_p\right) - \alpha_{bp}\beta_T n_b n_p\left(A\Delta L\right) \tag{2}$$

In steady-state, the particle-bubble collision efficiency of the mixing zone is obtained as follows [1]:

$$E_{cz} = \left(1-\frac{n_{p,e}}{n_{p,i}}\right) = \left[1-\exp\left(\frac{-\alpha_{pb}\left(\beta_{\text{perikinetic}}+\beta_{\text{orthokinetic}}\right)n_b L_{cz}}{U}\right)\right] \tag{3}$$

Perkinetic frequency is expressed as Eq. (4), in which k_B is the Boltzmann constant, T is the absolute temperature, and μ is the fluid viscosity [1,19].

$$\beta_{\text{perikinetic}} = \left(\frac{2k_B T}{3\mu}\right)\frac{\left(d_p+d_b\right)^2}{d_p d_b} \tag{4}$$

Orthokinetic aggregation in isotropic turbulence is expressed as Eq. (5), where ε is the average energy dissipation rate, and ϑ is the kinematic viscosity of the fluid [1,19].

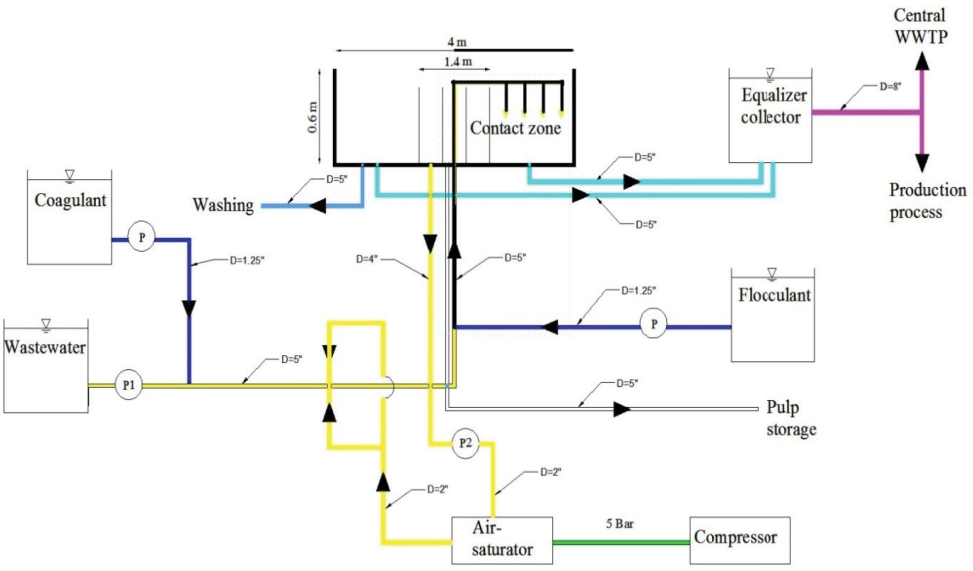

Fig. 2. Schematic illustration of the main pipe and four valves in RDAF.

$$\beta_{\text{orthokinetic}} = \frac{8\pi}{15}\left(R_p + R_b\right)^3\left(\frac{\varepsilon}{\vartheta}\right)^{1/2} \quad (5)$$

In conclusion, the general equation for particle-bubble collision efficiency of in the mixing zone is obtained as follows Eq. (6) [1,19]:

$$E_{cz} = \left[1 - \exp\left(\frac{-\alpha_{pb} n_b L_{cz}}{U}\left(\begin{array}{l} 3.9\times10^{-18}\dfrac{\left(d_p + d_b\right)^2}{d_p d_b} \\ +1.67\times10^{-18}\left(d_p + d_b\right)^3\left(\dfrac{\varepsilon}{\vartheta}\right)^{1/2}\end{array}\right)\right)\right] \quad (6)$$

2.2. Experimental data

Particle-bubble collision efficiency variables were obtained according to the following equations based on experimental data. These variables include the mass concentration in released air (C_b) and the saturator air concentration that can be expressed as the bubble number concentration (n_b) or the bubble volume concentration (ϕ_b) [12].

$$C_b = \frac{e\left(C_{\text{sat}} - C_{\text{fl}}\right)}{1+r} r \quad (7)$$

$$\varphi_b = \frac{C_b}{\rho_{\text{air}}} \quad (8)$$

$$n_b = \frac{6\varphi_b}{\pi\left(d_b\right)^3} \quad (9)$$

According to the operating scenarios of RDAF under study, the system is operated at two recycling flow rates: 0.48 and 0.38. Saturated air concentrations at these two rates are calculated as follows:

$$C_{b1} = \frac{e\left(C_{\text{sat}} - C_{\text{fl}}\right)}{1+r} r = \frac{0.7\left(127.5 - 5.5\right)}{1+0.48}0.48 = 27.7;$$
$$\varphi_{b1} = \frac{C_{b1}}{\rho_{\text{air}}} = 0.024$$

$$C_{b2} = \frac{e\left(C_{\text{sat}} - C_{\text{fl}}\right)}{1+r} r = \frac{0.7\left(127.5 - 5.5\right)}{1+0.38}0.38 = 23.5;$$
$$\varphi_{b2} = \frac{C_{b2}}{\rho_{\text{air}}} = 0.02$$

The air pressure operation in saturation is 3.5–4.5 bar, and according to the recycling flow rates, the diameter of the air bubbles is in the range of 60 to 100 μm. In this study, bubbles with diameters of 60, 80, and 100 μm were considered [1,4,12]. Thus, the number of bubbles at two recycling flow rates is calculated.

$$n_{b1,\min} = 4.6\times10^4; n_{b1,\text{ave}} = 8.96\times10^4;$$
$$n_{b1,\max} = 2.12\times10^5 \text{ bubble / mL}$$

$$n_{b2,\min} = 3.8\times10^4; n_{b2,\text{ave}} = 7.5\times10^4;$$
$$n_{b2,\max} = 1.77\times10^5 \text{ bubble / mL}$$

In a fully developed pipe flow, the turbulence intensity (T.I) at the core can be calculated with Eq. (10). The length scale and energy dissipation rate are estimated using Eq. (11) [46,47].

$$I = 0.16\times\text{Re}^{-1/8}; k = \frac{3}{2}I^2U^2; \varepsilon = C_\mu^{3/4}\frac{k^{3/2}}{l}; \text{OR } ; \varepsilon = 2.35\frac{k^{3/2}}{D} \quad (10)$$

where C_μ is 0.09.

$$\text{Re} = \frac{\rho U D}{\mu}; I = 0.16\times\text{Re}^{-1/8}; k = \frac{3}{2}I^2U^2 \text{ and } l = 0.07D \quad (11)$$

where $\varepsilon_1 = 3.3 \times 10^{-4}$ m^2/s^3; $\varepsilon_2 = 5.73 \times 10^{-4}$ m^2/s^3.

These data were used for determining the particle-bubble collision efficiency in the mixing zone.

2.3. ANSYS CFX R18.0

To simulate fluid flow, a widely used tool is ANSYS CFX R18.0 software, which solves fluid flow equations in a region with boundary conditions. The standard *k*–ε two-equation model is the most frequently used turbulence model for solving flow problems Eqs. (12) and (13). This model was employed in ANSYS CFX R18.0 [47].

$$\frac{\partial}{\partial t}\left(\rho k\right) + \frac{\partial}{\partial x_i}\left(\rho k U_i\right) = \frac{\partial}{\partial x_j}\left[\left(\mu + \frac{\mu_t}{\sigma_k}\right)\frac{\partial k}{\partial x_j}\right] + G_k - \rho\varepsilon \quad (12)$$

$$\frac{\partial}{\partial t}\left(\rho\varepsilon\right) + \frac{\partial}{\partial x_i}\left(\rho\varepsilon U_i\right) = \frac{\partial}{\partial x_j}\left[\left(\mu + \frac{\mu_t}{\sigma_\varepsilon}\right)\frac{\partial \varepsilon}{\partial x_j}\right] + C_1\frac{\varepsilon}{k}G_k - C_2\rho\frac{\varepsilon^2}{k} \quad (13)$$

2.4. The k–ε model

In the *k*–ε model, ε is the eddy dissipation rate of turbulence, at which the velocity fluctuations dissipate, and *k* is the turbulence kinetic energy defined as the variance of velocity fluctuations. By using this model, two new variables are added to the equations. Therefore, the continuity equation is expressed as Eq. (14) [47],

$$\frac{\partial \rho}{\partial t} + \frac{\partial}{\partial x_j}\left(\rho U_j\right) = 0 \quad (14)$$

and the momentum equation is expressed as Eq. (15) [47]:

$$\frac{\partial \rho U_i}{\partial t} + \frac{\partial}{\partial x_j}\left(\rho U_i U_j\right) = -\frac{\partial p'}{\partial x_i} + \frac{\partial}{\partial x_j}\left[\mu_{\text{eff}}\left(\frac{\partial U_i}{\partial x_j} + \frac{\partial U_j}{\partial x_i}\right)\right] + S_M \quad (15)$$

where S_M is the body forces sum, and μ_{eff} is the effective viscosity that takes the turbulence into account is expressed as Eq. (16) [47]:

$$\mu_{\text{eff}} = \mu + \mu_t \quad (16)$$

where μ_t is the viscosity of turbulence expressed as Eq. (17) [47]:

$$\mu_t = C_\mu \rho \frac{k^2}{\varepsilon} \quad (17)$$

3. Results and discussion

3.1. ANSYS CFX R18.0

Hydrodynamic parameters, including flow velocity in the mixing zone, as well as turbulence, were obtained by CFX R18.0. Fig. 3 shows the water velocity contours in the mixing zone in the first, second, third, and fourth operation scenarios.

Moreover, Fig. 4 shows the water turbulence in the mixing zone in each scenario. The velocities and turbulences obtained by ANSYS CFX were put in Eq. (6) and compared with experimental data.

3.2. Bubble-particle collision efficiency

The results indicated that the values of perkinetic frequency were very small; thus, its effect on the efficiencies could be ignored. Also, orthokinetic frequency was calculated as a function of turbulence, particle size, and bubble size in the valves and inserted in the collision efficiency model. In order to better evaluate the collision efficiencies, in all scenarios, the particle size is in the range of 50 to 300 μm. Fig. 5a shows the collision efficiency in the first scenario. In this case, the average length of the pipe was calculated as 1.8 m, the water velocity as 0.54 m/s, and the turbulence intensity as 0.00033 m^2/s^3. When the bubble size decreased from 100 to 60 μm, the efficiency reached approximately 100%. Particle collision efficiency for particles larger than 200 μm was close to 100%. Fig. 5b shows the collision efficiency in the second scenario. In this case, the average length of the pipe was obtained as 1.8 m, the water velocity as 0.68 m/s, and the turbulence intensity as

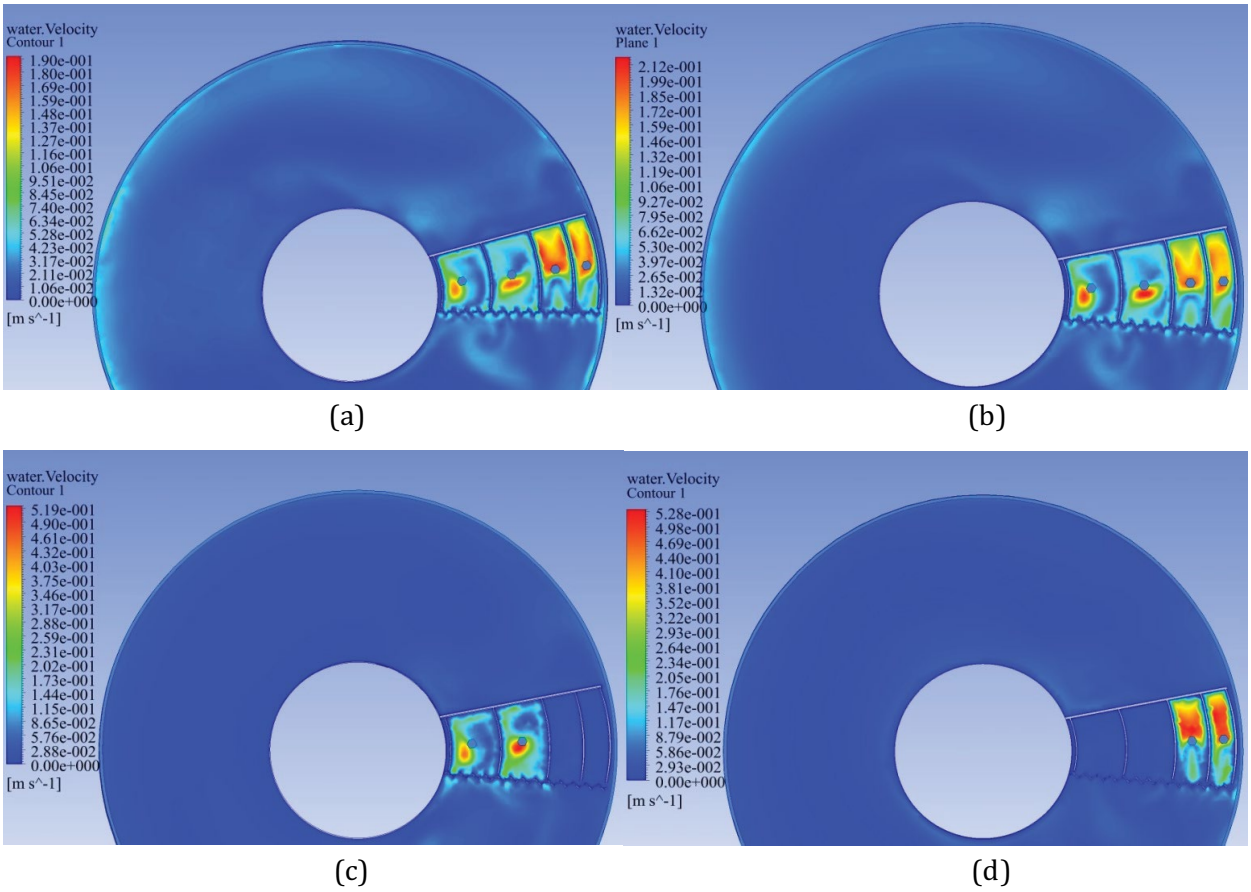

Fig. 3. Velocity in the pipe mixing zone when valves (a) 1#, 2#, 3#, 4#, (b) 1#, 2#, 3#, 4# (normal operation), (c) 1# and 2#, and (d) 3# and 4# are open.

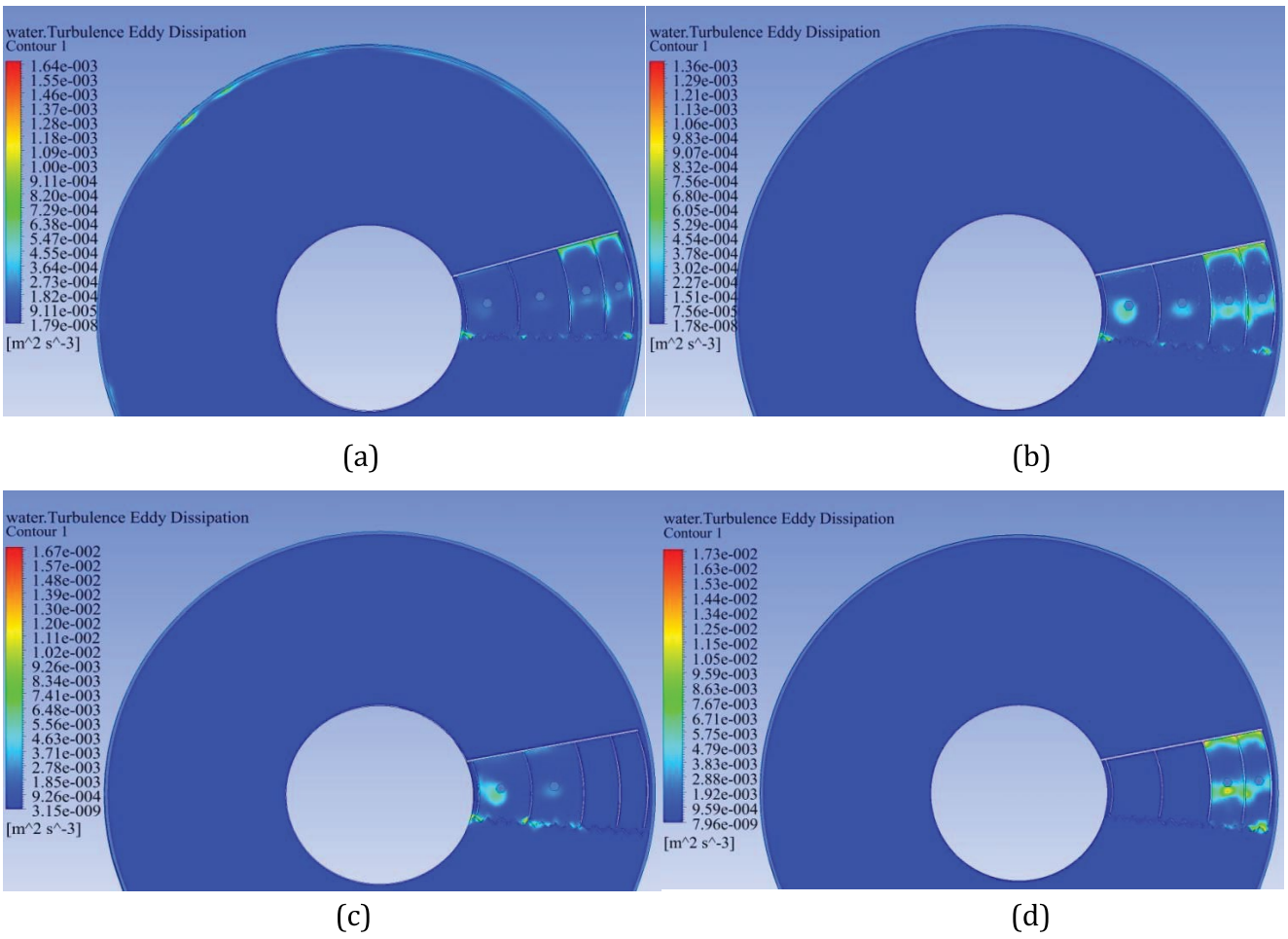

Fig. 4. Turbulence in the pipe mixing zone when: (a) 1#, 2#, 3#, 4#, (b) 1#, 2#, 3#, 4# (normal operation), (c) 1# and 2#, and (d) 3# and 4# are open.

0.00057 m^2/s^3. Particle collision efficiency of 100% for particles larger than 190 μm was obtained. When the bubble size decreased from 100 to 60 μm, an optimum efficiency of 100% was obtained. Fig. 5c shows the collision efficiency in the third scenario. In this case, the average length of the pipe was calculated as 1.77 m, water velocity as 0.68 m/s, and turbulence intensity as 0.00057 m^2/s^3. Particle collision efficiency for particles larger than 180 μm was close to 100%. By decreasing the bubble size from 80 to 60 μm, efficiency of 100% was reached. In addition, Fig. 5d shows the collision efficiency in the fourth scenario. In this scenario, the average length of the pipe was calculated as 2.3 m, water velocity as 0.68 m/s, and turbulence intensity as 0.00057 m^2/s^3. Particle collision efficiency for particles larger than 180 μm was close to 100%. The optimum particle size for 100% efficiency is 140 μm.

Edzwald and Haarhoff [1] proposed two good and poor coagulation factors and considered them in the modeling. In the first scenario in the mixing zone, shown in Fig. 6a, it is seen that at a good coagulation factor, (α = 0.5), a retention time of 5 s, and turbulence intensity of 0.0003 m^2/s^3, the efficiency is 65% for particles with a diameter of 50 μm, and by increasing the particle diameter, the efficiency approaches 100%. However, at a poor coagulation factor (α = 0.05), for particles with a diameter of 50 μm, the efficiency is 10%, and for particles with a diameter of up to 300 μm, the efficiency is 40%. After exiting the valves, the air bubbles expanded and discharged into the atmosphere.

Furthermore, in the second scenario shown in Fig. 6b, it is seen that at good coagulation (α = 0.5), a retention time of 4 s, and turbulence intensity of 0.00035 m^2/s^3, the efficiency is 75% for particles with a diameter of 50 μm. Moreover, by increasing the particle diameter, the efficiency approaches 100%. However, for a poor coagulation factor (α = 0.05), the efficiency is 5% for 50 μm particles, while the particle-bubble collision efficiency is 85% for particles with a diameter of up to 300 μm.

In Fig. 6c showing the third scenario, it is seen that at a good coagulation factor (α = 0.5), a retention time of 2 s, and a turbulence intensity of 0.0004 m^2/s^3, the efficiency is 55% for particles with a diameter of 50 μm, and as the particle diameter increases, the efficiency gradually reaches 100%. For a poor coagulation factor (α = 0.05), the efficiency is 8% for particles with a diameter of 50 μm, while the efficiency is 65% for particles up to 300 μm. Fig. 6d corresponding to the fourth scenario shows that at a good coagulation factor (α = 0.5), a retention time of 2 s, and a turbulence intensity of 0.00065 m^2/s^3, the efficiency is 65% for particles with a

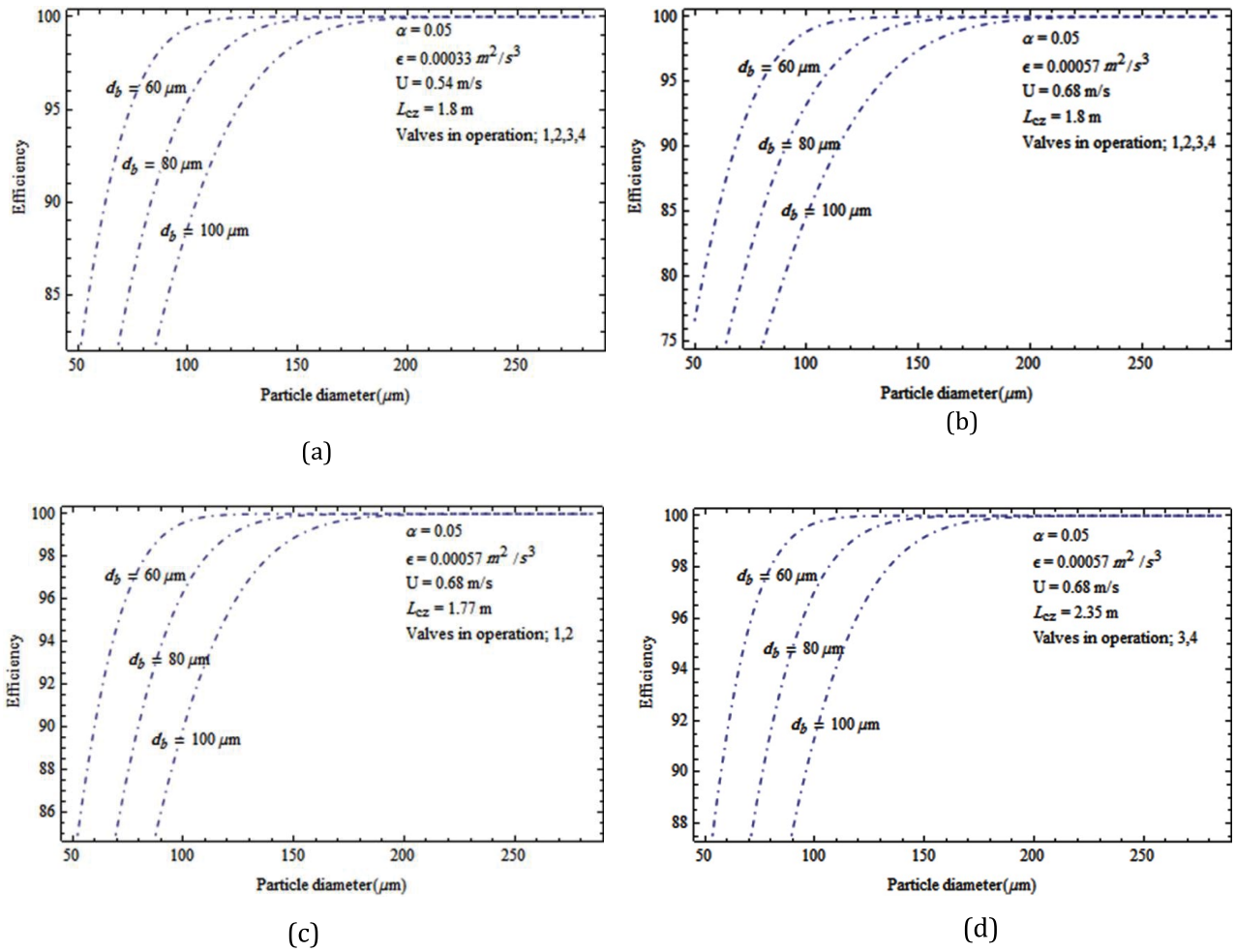

Fig. 5. Collision efficiency in the pipe mixing zone when valves (a) 1#, 2#, 3#, 4#, (b) 1#, 2#, 3#, 4# (normal operation), (c) 1# and 2#, and (d) 3# and 4# are open.

diameter of 50 μm, and as the particle size increases, the efficiency approaches 100% with a sharper gradient. In addition, for poor coagulation (α = 0.05), the efficiency is 10% for particles with a diameter of 50 μm, while it is 75% for particles of up to 300 μm in diameter. By combining the efficiencies in the pipe and mixing zone, the particle collision efficiency for each of the four modes of operation is 100%; however, in the second and fourth scenarios, according to hydrodynamic conditions, the production of particles is greater.

3.3. Particle size distribution test

The particle size test was performed in three scenarios out of the four scenarios except for the first scenario by the SLS method [42]. Sample points were selected at five points, including after valves, baffles, collector, slow rotating, and rapid rotating. The aim was to experimentally obtain particle size according to different turbulence and hydrodynamic conditions.

Three operating scenarios, except for the first scenario, were evaluated in the previous stage. To better compare the turbulence effect on the collision efficiency and size distribution of particles in the effluent, the particle size of the raw wastewater was determined as the basis for comparison with the subsequent changes. In the first scenario, valves #1 and #2 were opened. According to the measurements, the particle distribution was in the range of 0.283–399 μm. The obtained relative volume and diameter of the particles are the most important data of the particle size distribution. Fig. 7 shows that among the various operating modes, the rapid rotating mode can produce particles larger in diameter than the raw particles up to 563 μm, so this operating mode is recommended for higher operational efficiency. In other operating modes, turbulence may break down the particle to particles smaller compared with those in raw wastewater.

In the second scenario, valves #3 and #4 were opened. Fig. 8 shows that among the various operating modes, the slow rotating and after baffle modes can produce particles larger in diameter than the raw particles up to 1,124.7 μm; thus, these operating modes are recommended for higher operational efficiency. In this scenario, the operating modes often produce larger particle sizes than the raw wastewater particles, and there is a relatively uniform continuity and stability compared to the previous mode.

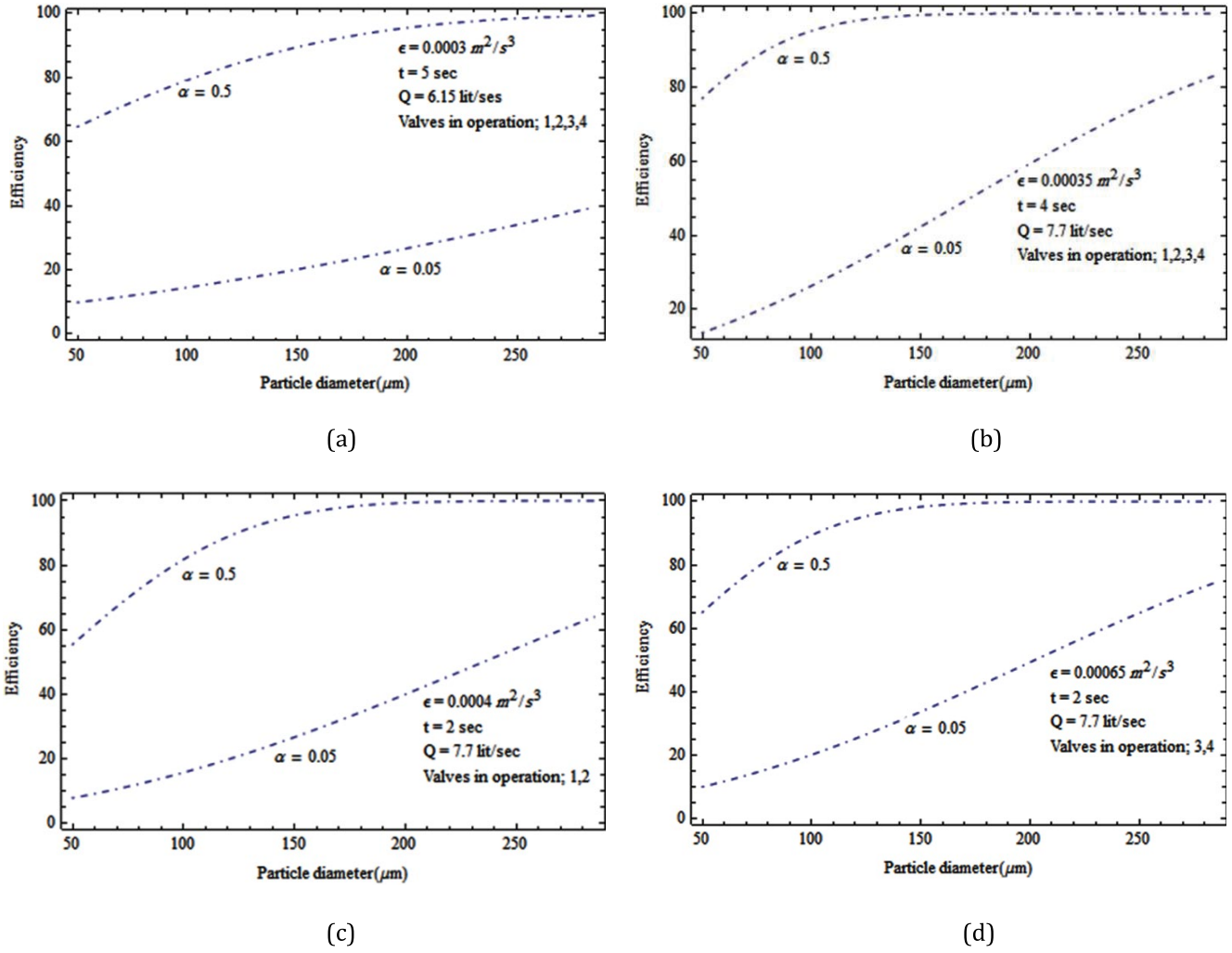

Fig. 6. Collision efficiency in the mixing zone when valves (a) 1#, 2#, 3#, 4#, (b) 1#, 2#, 3#, 4# (normal operation), (c) 1# and 2#, and (d) 3# and 4# are open.

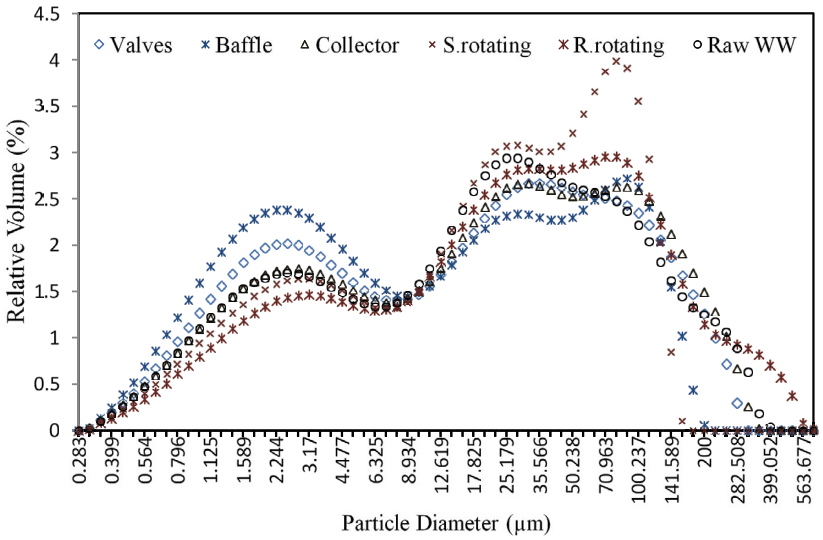

Fig. 7. Particle diameter when valves #1 and #2 are in operation.

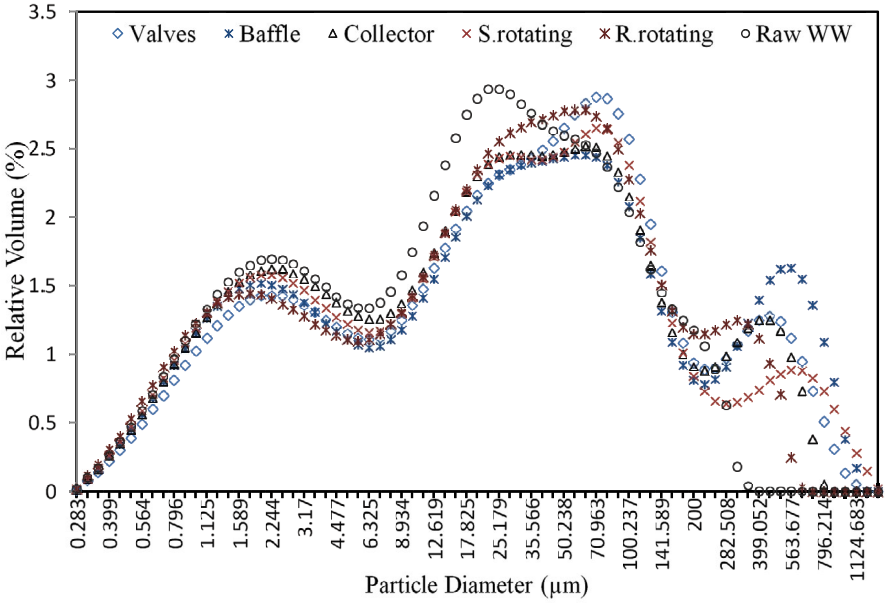

Fig. 8. Particle diameter when valves #3 and #4 are in operation.

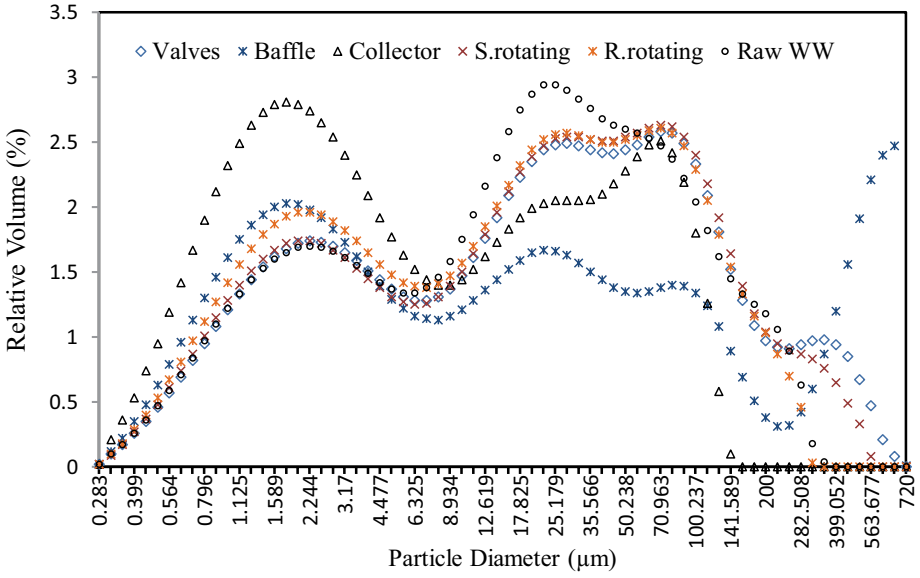

Fig. 9. Particle diameter when valves #1, #2, #3, and #4 are in operation.

In the last operation scenario, all the four valves were opened and considered with normal flow. Fig. 9 shows that the particle size increases to 720 µm in the post-valve and baffle modes. Especially after the baffle, the particle diameter continues to increase but decreases until the collector. This reduction in particle size may be due to turbulence within the separation zone. In comparison, among the three experimental scenarios presented, the second scenario resulted in the production of larger particle sizes up to several times the particle size of the raw wastewater with a higher correlation to the experimental modes. Therefore, this scenario can better increase RDAF system efficiency in terms of particle size and particle removal efficiencies.

4. Conclusions

In this study, particle collision efficiency was investigated using ANSYS CFX R18.0, mathematical modeling, and experimental analysis to predict the effect of turbulence on collisions in the mixing zone of an industrial RDAF in Rangin Kaghaz-e-Khazar Co., Iran. As discussed in the paper, the particle-bubble collision efficiency is based on transport and attachment and do not depend on the geometry in DAF systems (circular and rectangular). Thus, the results of this research can be extended to all DAF systems. According to the SLS test, a particle size range of 50–300 µm was considered. Four scenarios at two

mixing zones were considered for RDAF operation. The first mixing zone was the particle-bubble collision inside the pipe. In the first case, for the corresponding hydrodynamic conditions, the collision efficiency of particles with a diameter greater than 200 μm was 100%. In the second case, for particles larger than 190 μm, the particle collision efficiency was 100%. In the third case, the particle diameter was 180 μm, and in the fourth case, the optimal particle diameter was 140 μm. In the next mixing zone, four scenarios were examined. In all the four scenarios, for particles with a diameter of 50 μm and above and poor coagulation conditions, the efficiency of particle-bubble collisions was higher than 10%. By increasing the particle diameter up to 300 μm, the particle-bubble collision efficiency in the second mixing zone reached 40% to 80%, which was in the weak coagulation state. In addition, the collision efficiencies were higher for coagulations with higher alpha values.

The particle size distribution test was performed for the three scenarios by the SLS method. Sampling was conducted at five points. SLS test was performed for two purposes: detecting particle size in raw wastewater and validating of experimental and mathematical models. Based on that, the particle size was considered from 0.283 to around 300 μm with different relative volumes. Of the four scenarios considered in the previous section, three operating scenarios were considered in this section, except the first scenario. The highest particle diameters were related to the scenario in which valves 3 and 4 were open and valves 1 and 2 were closed, and the hydrodynamic conditions related to those particles were up to 1,120 μm in diameter. Conversely, when valves 1 and 2 were open, the maximum output particle diameter was 563 μm.

Author declarations

Funding

The authors declare that no funds, grants, or other support were received during the preparation of this manuscript.

Conflicts of interest

The authors have no relevant financial or non-financial interests to disclose.

Availability of data and material

Some or all data, models, or code that support the findings of this study are available from the corresponding author upon reasonable request.

Code availability

ANSYS CFX R.18.0 used for this research.

Author contributions

All authors, A.H.J, H.A.R, S.M.B, M.V. and R.R., contributed to the study conception and design. The first draft of the manuscript was written by all authors and they commented on previous versions of the manuscript. All authors read and approved the final manuscript.

Symbols

A	—	Area
C	—	Concentration
CFD	—	Computational fluid dynamics
D	—	Diameter
dt	—	Time step
e	—	Efficiency
E_{cz}	—	Contact zone efficiency
K	—	Coefficient
k_B	—	Boltzmann constant
L	—	Length
L	—	Length scale
L_{cz}	—	Length of contact zone
N_{ij}	—	Overall particle growth rate
n	—	Number
PSD	—	Particle size distribution
Q	—	Flow rate
Q_r	—	Recycle flow
R	—	Radius
r	—	Recycle ratio
RDAF	—	Rotating dissolved air flotation
Re	—	Reynolds
SLS	—	Static light scattering
S_M	—	Body forces sum
T	—	Absolute temperature
T.I	—	Turbulence intensity
U	—	Velocity

Greek

ρ	—	Density
μ	—	Dynamic viscosity
υ	—	Kinematic viscosity
K	—	Turbulence kinetic energy
ε	—	Turbulence eddy dissipation rate
σ_k	—	Constant
ϕ_b	—	Bubble volume concentration
C_b	—	Bubble concentration
C_μ	—	Constant
α_{ij}	—	Collision efficiency factor
β_{ij}	—	Collision mechanism
$\beta_{perkinetic}$	—	Perkinetic frequency
$\beta_{orthokinetic}$	—	Orthokinetic frequency

Subscripts

b	—	Bubble
p	—	Particle
i	—	Bubble; X direction
j	—	Particle; Y direction

References

[1] J.K. Edzwald, J. Haarhoff, Dissolved Air Flotation for Water Clarification, McGraw-Hill Companies: American Water Works Association, North America, 2011.
[2] Krofta, Proven Solutions in Liquid-Solid Separation, Krofta® Dissolved Air Flotation, Krofta a Waterleau Company, Dalton, MA 01227, USA, 2015.
[3] R. Miranda, I. Latour, A. Blanco, Understanding the efficiency of aluminum coagulants used in dissolved air flotation (DAF), Front. Chem., 8 (2020), doi: 10.3389/fchem.2020.00027.

[4] L.K. Wang, N.K. Shammas, W.A. Selke, D.B. Aulenbach, Eds., Flotation Technology, Handbook of Environmental Engineering, Humana Press, Spring Street, New York, NY 10013, USA, Vol. 12, 2010.
[5] Rangin Kaghaz-e-Khazar, Co., The Operational Records for One Decade in Paper-Recycling Mill in Northern of Iran, Rangin Kaghaz-e-Khazar, Rajeh Industrial Town, Iran, 2020.
[6] A. Hasannattaj Jelodar, H. Amini Rad, S.M. Borghei, M. Vossoughi, R. Rouhollahi, Particle removal optimization in rotating dissolved air flotation used in paper-recycling wastewater treatment, Water Environ. J., 36 (2022) 3–17.
[7] H.A. Oliveira, A.C. Azevedo, R. Etchepare, J. Rubio, Separation of emulsified crude oil in saline water by flotation with micro- and nanobubbles generated by a multiphase pump, Water Sci. Technol., 76 (2017) 2710–2718.
[8] Z. Amjad, The Science and Technology of Industrial Water Treatment, Taylor and Francis Group, IWA Publishing, London SW1H 0QS, UK, 2010.
[9] M.M. Benjamin, D.F. Lawler, Water Quality Engineering: Physical/Chemical Treatment Processes, John Wiley & Sons, Inc., Hoboken, New Jersey, 2013.
[10] G.Z. Kyzas, K.A. Matis, Flotation in water and wastewater treatment, Processes, 6 (2018) 116, doi: 10.3390/pr6080116.
[11] A. Chen., Z. Wang., J. Yang, Influence of bubble size on the fluid dynamic behavior of a DAF tank: a 3D numerical investigation, Colloids Surf., A, 495 (2016) 200–207.
[12] A. Bahadori, G. Zahedi, S. Zendehboudi, M. Bahadori, Estimation of air concentration in dissolved air flotation (DAF) systems using a simple predictive tool, Chem. Eng. Res. Des., 91 (2013) 184–190.
[13] J. Behin, S. Bahrami, Modeling an industrial dissolved air flotation tank used for separating oil from wastewater, Chem. Eng. Process. Process Intensif., 59 (2012) 1–8.
[14] M. Han, T. Kim, D. Kwak, Measurement of bubble bed depth in dissolved air flotation using a particle counter, J. Water Supply Res. Technol. AQUA, 58 (2009) 57–63.
[15] S.A. Hussain, A. Idris, Spiral motion of air bubbles in multiphase mixing for wastewater treatment, Procedia Eng., 148 (2016) 1034–1042.
[16] S. Li, K. Jue, C. Sun, Effect of bubble surface properties on bubble–particle collision efficiency in froth flotation, Minerals, 10 (2020) 367, doi: 10.3390/min10040367.
[17] S. Li, M. Philip Schwarz, Y. Feng, P. Witt, C. Sun, A CFD study of particle–bubble collision efficiency in froth flotation, Miner. Eng., 141 (2019) 105855, doi: 10.1016/j.mineng.2019.105855.
[18] M. Bondelind, S. Sasic, M. Kostoglou, L. Bergdahl, T.J.R. Pettersson, Single- and two-phase numerical models of dissolved air flotation: comparison of 2D and 3D simulations, Colloids Surf., A, 365 (2010) 137–144.
[19] J. Bridgeman, B. Jefferson, S.A. Parsons, Computational fluid dynamics modelling of flocculation in water treatment: a review, Eng. Appl. Comput. Fluid Mech., 3 (2009) 220–241.
[20] R. Bürger, S. Diehl, C. Martí, Y. Vásquez, Simulation and control of dissolved air flotation and column froth flotation with simultaneous sedimentation, Water Sci. Technol., 81 (2020) 1723–1732.
[21] K. Satpathy, U. Rehman, B. Cools, L. Verdickt, G. Peleman, I. Nopens, CFD-based process optimization of a dissolved air flotation system for drinking water production, Water Sci. Technol., 81 (2020) 1668–1681.
[22] V.A. Emmanouil, T.D. Karapantsios, K.A. Matis, Two and three-phase simulations of an ill-functioning dissolved air flotation tank, Int. J. Environ. Waste Manage., 8 (2011) 215–228.
[23] V. Emmanouil, E.P. Skaperdas, T.D. Karapantsios, K.A. Matis, Two-phase simulations of an off-nominally operating dissolved-air flotation tank, Int. J. Environ. Pollut., 30 (2007) 213–230.
[24] Y.L. Wang, N. Wang, R. Jia, K. Zhang, B. Liu, W. Song, J. Jia, Research on CFD numerical simulation and flow field characteristics of countercurrent–cocurrent dissolved air flotation, Water Sci. Technol., 77 (2018) 1280–1292.
[25] Y. Wang, X. Jin, S. Yang, G. Wang, L. Xu, P. Jin, X. Shi, Y. Shi, Interactions between flocs and bubbles in the separation zone of dissolved air flotation system, Sci. Total Environ., 761 (2021) 143222.
[26] F. Bloom, T.J. Heindel, Modeling flotation separation in a semi-batch process, Chem. Eng. Sci., 58 (2003) 353–365.
[27] B. Deng, Q. Ding, D. Ge, Three dimensional Eulerian-Eulerian simulation on hydrodynamics in dissolved air flotation tank with different turbulence models, Water Sci. Technol., 76 (2017) 425–433.
[28] M. Bondelind, S. Sasic, L. Bergdahl, A model to estimate the size of aggregates formed in a dissolved air flotation unit, Appl. Math. Modell., 37 (2013) 3036–3047.
[29] H. Ström, M. Bondelind, S. Sasic, A novel hybrid scheme for making feasible numerical investigations of industrial three-phase flows with aggregation, Ind. Eng. Chem. Res., 52 (2013) 10022–10027.
[30] D.-H. Kwak, M.-S. Kim, Estimation and evaluation of auto-flocculated algae harvesting efficiency using the population balance in turbulence model in flotation process, Water Sci. Technol., 77 (2018) 1165–1178.
[31] F. Julien Saint Amand, Hydrodynamics of deinking flotation, Int. J. Miner. Process, 56 (1999) 277–316.
[32] F. Bloom, T.J. Heindel, On the structure of collision and detachment frequencies in flotation models, Chem. Eng. Sci., 57 (2002) 2467–2473.
[33] R.B. Moruzzi, M.A.P. Reali, The influence of floc size and hydraulic detention time on the performance of a dissolved air flotation (DAF) pilot unit in the light of a mathematical model, Bioprocess Biosyst. Eng., 37 (2014) 2445–2452, doi: 10.1007/s00449-014-1221-6.
[34] V.R. Fanaie, M. Khiadani, Effect of salinity on air dissolution, size distribution of microbubbles, and hydrodynamics of a dissolved air flotation (DAF) system, Colloids Surf., A, 591 (2020) 124547, doi: 10.1016/j.colsurfa.2020.124547.
[35] B. Shahbazi, B. Rezai, The effect of micro turbulence on quartz flotation rate, Iran. J. Chem. Chem. Eng., 34 (2015) 79–89.
[36] T.Y. Liu, P.T.L. Koh, M.P. Schwarz, CFD-Based Modelling of Bubble-Particle Collision Efficiency with Mobile Bubble Surface in a Turbulent Environment, Fifth International Conference on CFD in the Process Industries, CSIRO Minerals, Melbourne, Australia, 2006.
[37] M. Kostoglou, T.D. Karapantsios, K.A. Matis, Modeling local flotation frequency in a turbulent flow field, Adv. Colloid Interface Sci., 122 (2006) 79–91.
[38] M. Kostoglou, T.D. Karapantsios, K.A. Matis, CFD model for the design of large scale flotation tanks for water and wastewater treatment, Ind. Eng. Chem. Res., 46 (2007) 6590–6599.
[39] B. Lakghomi, Y. Lawryshyn, R. Hofmann, Importance of flow stratification and bubble aggregation in the separation zone of a dissolved air flotation tank, Water Res., 46 (2012) 4468–4476.
[40] B. Lakghomi, Y. Lawryshyn, R. Hofmann, A model of particle removal in a dissolved air flotation tank: importance of stratified flow and bubble size, Water Res., 68 (2015) 262–272.
[41] B. Lakghomi, Y. Lawryshyn, R. Hofmann, Evaluation of flow hydrodynamics in a pilot-scale dissolved air flotation tank: a comparison between CFD and experimental measurements, Water Sci. Technol., 72 (2015) 1111–1118.
[42] Standard Methods for the Examination of Water and Wastewater, 23rd ed., American Public Health Association, American Water Works Association, Water Environment Federation, Washington DC, USA, 2017.
[43] J.K. Edzwald, Dissolved air flotation and me, Water Res., 44 (2011) 2077–2106.
[44] E. Antunes, F.A.P. Garcia, P. Ferreira, A. Blanco, C. Negro, M.G. Rasteiro, Modelling PCC flocculation by bridging mechanism using population balances: effect of polymer characteristics on flocculation, Chem. Eng. Sci., 65 (2010) 3798–3807.
[45] G. Heng Yeoh, C.P. Cheung, J. Tu, Multiphase Flow Analysis Using Population Balance Modeling Bubbles, Drops and Particles, Elsevier Ltd., 2014.
[46] M. Ahsan, Numerical analysis of friction factor for a fully developed turbulent flow using k–ε turbulence model with enhanced wall treatment, Beni-Suef Univ. J. Basic Appl. Sci., 3 (2014) 269–277.
[47] ANSYS, ANSYS CFX-Solver Modeling Guide, ANSYS Inc., U.S.A., 2017.